ACS OMEGA

Open Access

http://pubs.acs.org/journal/acsodf

Article

Unveiling Hydrogen Bonding and Solvent Effects on Directed Nitrile Oxide [3 + 2] Cycloaddition Reactions: Selectivity of 2,2-Dimethylpropane Nitrile Oxide with Cyclopentenylbenzamide: An MEDT Study

Sofiane Benmetir,* Lakhdar Benhamed, Noureddine Tchouar, Haydar Mohammad-Salim,* Jesús Vicente de Julián-Ortiz, Mar Ríos-Gutiérrez, and Luis R. Domingo

Cite This: *ACS Omega* 2025, 10, 13868−13879

Read Online

ACCESS | Metrics & More | Article Recommendations | Supporting Information

ABSTRACT: The role of hydrogen bond and solvent effects on the regio- and diastereoselectivity of the [3 + 2] cycloaddition reaction (32CA) between 2,2-dimethylpropanenitrile oxide (NO) and *N*-(cyclopent-2-en-1-yl)benzamide has been theoretically studied at the B3LYP/6-311++G(d,p) level using the molecular electron density theory (MEDT). Solvent effects of dichloromethane (DCM) and benzene were taken into account. The electron localization function (ELF) classifies NO as a three-atom component with a zwitterionic electronic structure, which participates in zwitterionic-type 32CA reactions. The reactions occur through a one-step mechanism and present high activation Gibbs free energies in DCM and in benzene, with a slight difference favoring the reaction in benzene. Along the intrinsic reaction coordinate reaction pathway, the topological analysis of the ELF shows the asynchronous formation of the C−C bond prior to the C−O bond by coupling the two-carbon pseudoradical centers. The low global electron density transfer indicates that these reactions have a nonpolar character, which accounts for their high Gibbs free activation energies. Analysis of the noncovalent interactions associated with the TSs reveals a hydrogen bond in the favored TS, which confirms its participation in the experimental selectivities.

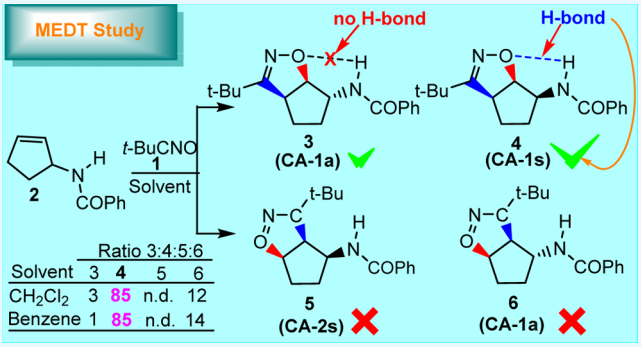

1. INTRODUCTION

The concept of [3 + 2] cycloaddition (32CA) was initially suggested by Smith in 1938.[1] This reaction became widely applicable only after its generalization by Huisgen in the 1960s.[2] The 32CA reactions, defined by the interaction between a three-atom component (TAC)[3] and an olefin, offer a very important method to prepare five-membered ring heterocycles.[4] 32CA reactions have become versatile strategies for chemo-, regio-, and stereoselective synthesis in organic chemistry.[5−8] These reactions are also increasingly studied by chemists for their possibility to give heterocyclic compounds in pharmacology.[9−11] As one of the many TACs used in these cycloaddition reactions, nitrile *N*-oxides (NOs)[12−14] particularly lead to isoxazole and isoxazoline frameworks[4,15] when reacting with an appropriate ethylene or acetylene derivative, respectively. Due to the stupendous chemical properties of isoxazoline compounds, making it more useful in many domains, various studies have been extensively investigated in the recent years.[16−28] In the drug discovery process, organic compounds containing an isoxazoline unit as the core are known by their biological activities as antibacterial,[16,19,20] antifungal,[16,20−22] analgesic,[16,29,30] anti-inflammatory,[16−18,20] antitumoral,[16,20,23,24,27,29] and antiviral.[16,20,25−27,29] In the industry, isoxazoline derivatives can also be used as chemical substances in agronomy and in dyes,[16,31] electrical insulating oils, and high-temperature lubricants.[28]

The application of the 32CA reactions for synthesizing isoxazoline compounds has shown an increasing interest in the theoretical sciences.[32−43] The study of chemical reactions is considered incomplete without the combination of experimental data and theoretical results. In addition to the design of appropriate reaction conditions, theoretical studies of the 32CA reactions enable also to provide information about the selectivity of these processes. Particularly, the molecular electron density theory (MEDT)[44] allows establishing the importance of the change in electron densities through the reaction paths.[45,46] 32CA reactions of NOs with quiral alkene

Received: August 23, 2024
Revised: February 21, 2025
Accepted: February 26, 2025
Published: April 3, 2025

https://doi.org/10.1021/acsomega.4c07794
ACS Omega 2025, 10, 13868−13879

Scheme 1. Solvent Effects on the 32CA Reaction of 2,2-Dimethylpropanenitrile Oxide (1) with *N*-(Cyclopent-2-en-1-yl)benzamide (2)

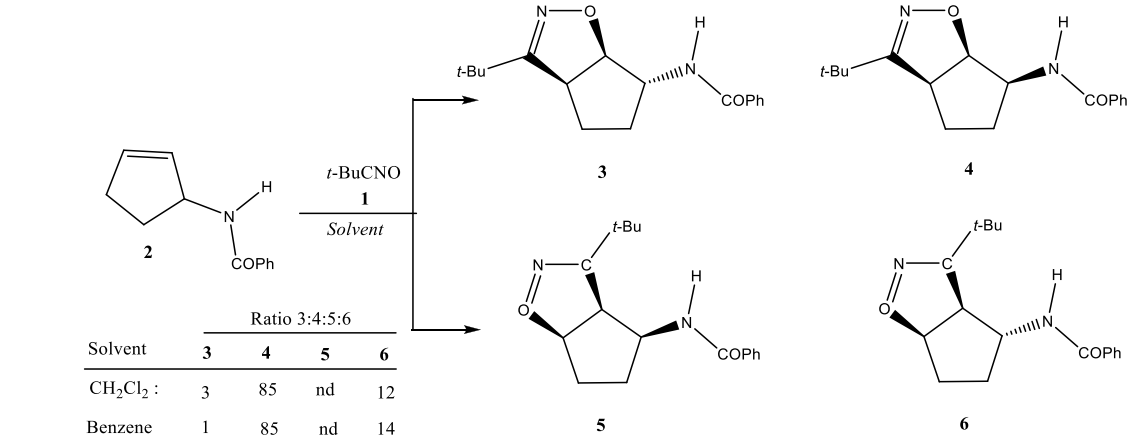

Scheme 2. Regioisomeric and Stereoisomeric Reaction Pathways along the 32CA Reaction of 2,2-Dimethylpropanenitrile Oxide (1) with *N*-(Cyclopent-2-en-1-yl)benzamide (2)

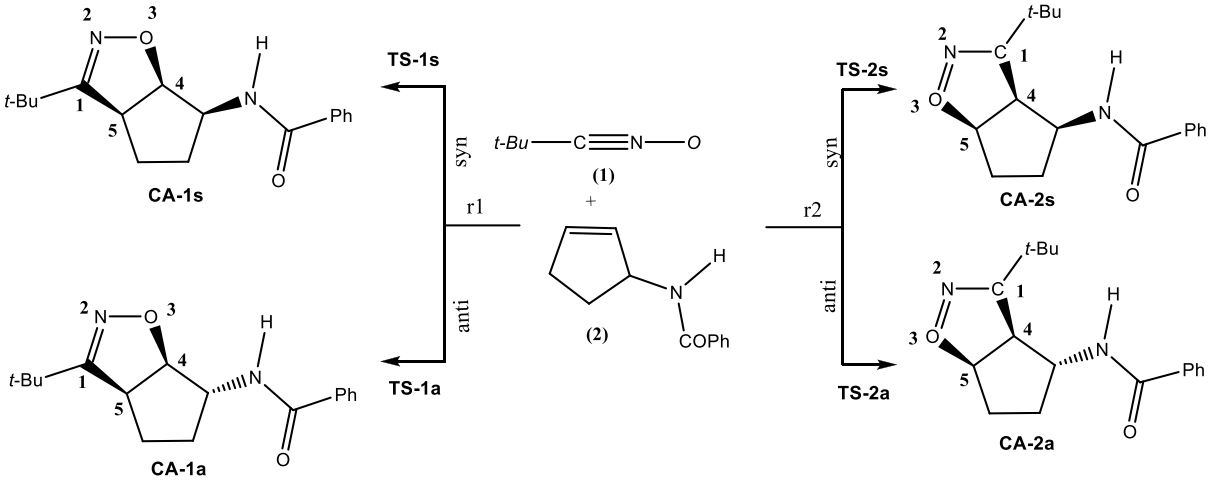

derivatives present, in general, experimental total regioselectivity and stereoselectivity resulting from the attack of NO to one of the two diastereotopic faces of the olefin C=C bond. The application of MEDT has allowed classifying these reactions as zwitterionic type (zw-type), in which NO (TAC) is present, usually, a zwitterionic structure. This type of reactions usually present high activation energies and demand the use of adequate nucleophilic/electrophilic interactions to take place easily[3]

In 1990, by studying a series of simple 3-cyclopentenylamides as reagents toward NOs, Curran et al. [*J. Org. Chem.* **1990**, 55(12), p. 3710−3712] found that the relatively acidic hydrogen of secondary amides could control both the regio- and stereochemistry in 32CA reactions of NOs. They mentioned that NOs added preferentially on the opposite (*anti*) face of the alkene, indicating that a hydrogen bond is probably operating, and the predominant cycloadduct formation is supported for a hydrogen-bond-directed NO 32CA reaction. Moreover, to test whether solvents could disrupt the hydrogen bond between the NOs and 3-cyclopentenylamides, dichloromethane (DCM) and benzene were included, finding that the product ratios and conversion percent's do not depend strongly on the solvent.

The purpose of our work in this paper is to achieve an MEDT investigation of the 32CA reaction between 2,2-dimethylpropanenitrile oxide (**1**) and *N*-(cyclopent-2-en-1-yl)benzamide (**2**) (Scheme 1), in order to gain insights on the mechanism, selectivity, and role of the hydrogen bond formation and solvent effects on this 32CA reaction experimentally studied.[47] For that, all competitive pathways of this 32CA reaction were examined and studied. These are named *r*1/*r*2 regioselective reaction paths and *syn*/*anti* diastereoisomeric approach modes.

2. COMPUTATIONAL DETAILS AND METHODOLOGY

All DFT calculations reported in this paper were realized using B3LYP[48,49] as an exchange−correlation functional, with the 6-311++G(d,p) basis set,[50] implemented in the Gaussian 09 program.[51] The optimization of stationary points was carried out using the Berny analytical gradient optimization method.[52,53] To verify if TSs have only one imaginary frequency, the stationary points were characterized by frequency computations and visualized using the CYLView program.[54] For all optimized transition states, using the second-order González−Schlegel integration method,[55,56] the calculations of the intrinsic reaction coordinate (IRC)[57] have been effectuated in order to verify that the located TSs are

https://doi.org/10.1021/acsomega.4c07794
ACS Omega 2025, 10, 13868−13879

associated with the reagents and cycloadducts as minimum stationary points. The effect of solvents is taken in account using the polarizable continuum model (IEFPCM) developed by the group of Tomasi et al.[58−60] in the framework of the self-consistent reaction field.[61−63] Based on Gibbs free energy differences, the Maxwell−Boltzmann populations, proportional to $e^{-\Delta G_O/RT}$, was calculated for all of associated transition states and the corresponding cycloadducts in DCM and benzene as solvents. At the TSs, the global electron density transfer (GEDT)[64] was calculated basing on natural population analysis.[65,66] The formula is given by GEDT (f) = $\sum_{q\in f} q$,[64] where the sign shows indications about the direction of the flux; the positive values denote a flux from the considered framework toward the other. Basing on conceptual density functional theory, the global indices of reactivity,[67,68] namely, chemical hardness (η), electronic chemical potential (μ), electrophilicity (ω), and relative nucleophilicity (N), were calculated according to the formulas given in ref 69. The electron localization function (ELF) topological studies were carried out for the most significant points of the potential energy surface (PES) curve using the Multifwn program.[70] Finally, the bond strength of the hydrogen bond was evaluated using noncovalent interactions[71−75] (NCIs), which allows a visualization of these NCIs using the electron density of the system.

3. RESULTS AND DISCUSSION

3.1. PES Study of the 32CA Reaction of NO (1) and Ethylene (2). Due to the nonsymmetric structure of ethylene (**2**) and the linear structure of the nitrile oxide (**1**), four different competitive reaction paths are feasible (see Scheme 2). These reaction paths can proceed through two possible regioisomeric approach modes, *r*1/*r*2, and two diastereoisomeric approach modes, *anti*/*syn*. As solvent effects[76−78] on the 32CA reaction are experimentally considered,[47] all calculations were realized in the gas phase and also in solvents. The four TSs localized and characterized are denoted: **TS-1s**, **TS-1a**, **TS-2s**, and **TS-2a**, and the corresponding isoxazoline cycloadducts are denoted: **CA-1s**, **CA-1a**, **CA-2s**, and **CA-2a**, respectively (see Scheme 2). The relative energies in the gas phase and the relative Gibbs free energies in DCM and in benzene are gathered in Table 1.

Table 1. Gas-Phase Relative Energies (ΔE) and Solvent-Phase Relative Gibbs Free Energies ($\Delta G°$) Corresponding to the Possible Paths, Calculated on B3LYP/6-311++G(d,p) in kcal mol^{-1}[a]

	gas phase	in DCM		in benzene	
species	ΔE[b]	$\Delta G°$[b]	pop. (%)	$\Delta G°$[b]	pop. (%)
TS-1s	**18.0**	**34.4**	**79.5**	**33.7**	**56.6**
TS-1a	19.9	36.3	3.3	35.2	6.9
TS-2s	20.2	38.0	0.1	36.5	0.4
TS-2a	19.0	35.4	17.1	34.3	36.1
CA-1s	**−31.6**	**−11.9**	**66.9**	**−12.4**	**67.0**
CA-1a	−29.5	−11.2	33.0	−11.4	32.8
CA-2s	−27.6	−7.4	0.0	−7.6	0.0
CA-2a	−28.4	−8.7	0.1	−9.2	0.2

[a]Maxwell−Boltzmann populations are given in %. [b]Relative to reactants (**1** + **2**).

The activation and reaction energies calculated at the B3LYP/6-311++G(d,p) level (Table 1) show, clearly, that the *r*1/*syn* reaction pathway yielding to the **CA-1s** cycloadduct formation, via **TS-1s**, is favored kinetically and thermodynamically. Note that **TS-1s** is located, in the gas phase, at 18.0 kcal mol^{-1} above reactants. It is also the lowest one, with calculated activation Gibbs free energies of 34.4 and 33.7 kcal mol^{-1} in DCM and benzene, respectively. The Gibbs free energy difference between regioisomeric **TS-1s** and **TS-2s** is 2.8 kcal mol^{-1}, indicating a high *r*1 regioselectivity, while that between **TS-1s** and **TS-1a** is 1.5 kcal mol^{-1}, showing a relatively high *syn* diastereoselectivity as well. Furthermore, the calculated Maxwell−Boltzmann populations confirm the predominance of **TS-1s** and **TS-2a** by 79.5% and 17.1% in DCM and by 56.6% and 36.1% in benzene, respectively. **TS-1a** shows only 3.3% and 6.9% in DCM and benzene, respectively, while the population of **TS-2s** is negligible, emphasizing that the *r*1/*syn* reaction is, kinetically, the most favored pathway. Consequently, the calculated reaction Gibbs free energies show that the formation of the favored **CA-1s** cycloadduct, via *r*1/*syn* path, is the most exergonic reaction by −11.9 kcal mol^{-1} in DCM and −12.4 kcal mol^{-1} in benzene. Hence, **CA-1s** is, thermodynamically, the most favored cycloadduct with a population of around 67% in both solvents (Table 1). These results clearly show that **CA-1s**, occurred via the *r*1/*syn* reaction pathway, is the major adduct as observed experimentally.[47] Note that using the benzene as the solvent leads to a slight diminution of approximately 0.5 kcal mol^{-1} in the TS and cycloadduct energies compared to DCM. In Figure 1, the 32CA reaction profiles between NO (**1**) and alkene (**2**) in benzene are presented.

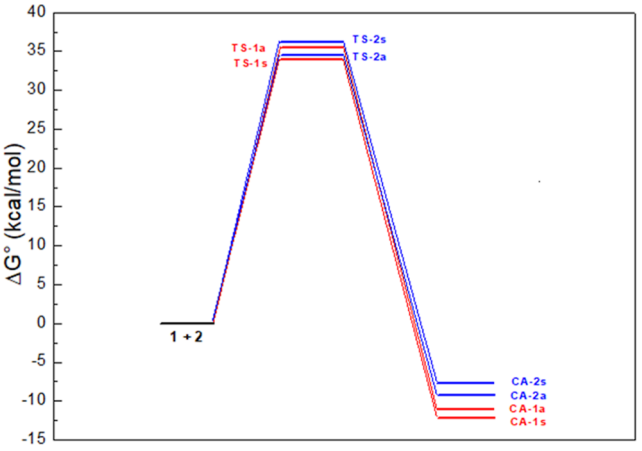

Figure 1. B3LYP/6-311++G(d,p) profiles of the 32CA reaction paths between NO (**1**) and ethylene (**2**), computed in benzene (the profiles in DCM are shown in the Electronic Supporting Information).

From the results of B3LYP/6-311++G(d,p) calculations given in Table 1, we conclude that the *r*1-favored regioselective path corresponds to the C1−C5 and O3−C4 bond formations; NO is added on the same face of the ethylene as the amide (*syn*) (see Scheme 2).

The four TS geometries, corresponding to the four possible pathways, are visualized in CYLview[79] and given in Figure 2. However, the Cartesian coordinates of reactants, TSs, and cycloadducts optimized in the gas phase, in DCM, and in benzene, are given in the Electronic Supporting Information. At the *syn* transition states, the distances between interacting

https://doi.org/10.1021/acsomega.4c07794
ACS Omega 2025, 10, 13868−13879

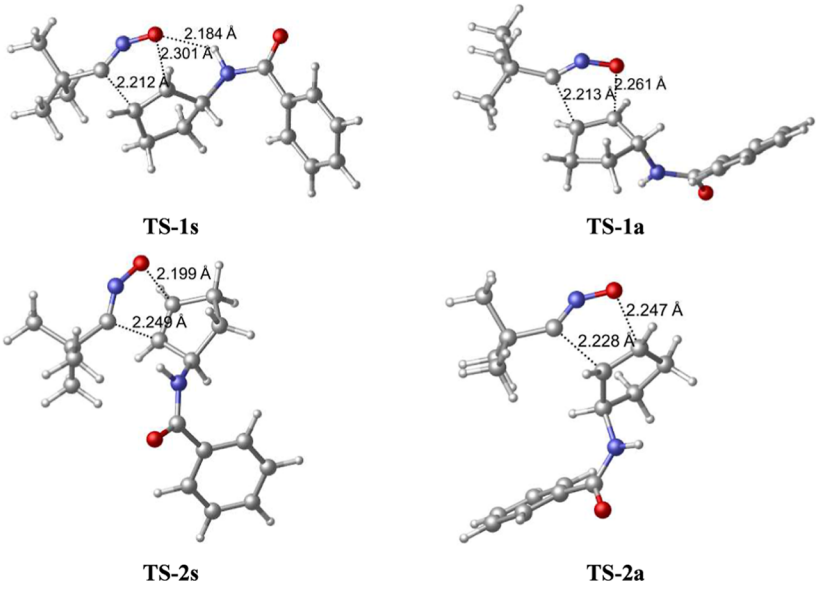

Figure 2. Structures of TSs associated with the 32CA reaction of NO (**1**) with ethylene (**2**), optimized in the gas phase at the B3LYP/6-311++G(d,p) level.

atoms in C1−C5 and O3−C4 are, respectively, 2.212 and 2.301 Å at **TS-1s** and 2.249 and 2.199 Å at **TS-2s**. However, at the *anti* TSs, the distances in C1−C4 and O3−C5 are, respectively, 2.213 and 2.261 Å at **TS-1a** and 2.228 and 2.247 Å at **TS-2a** (Figure 4). The present distances point out a geometrical asynchronicity. The asynchronous process is also observed in bond formations, in which C1−C5 is more advanced than the O3−C4 at **TS-1s**. The presence of a hydrogen bonding N−H···O of 2.184 Å at **TS-1s**, discussed in more detail below in Section 3.5, may favor the *r*1/*syn* path (see Figure 2).

The GEDT analysis at the TSs, in both solvents, shows a small transfer of electron density from the NO to the ethylene frameworks, 0.05 e. This very small value reveals that the 32CA reaction between NO (**1**) and ethylene (**2**) has a nonpolar character, which is a consequence of the slight difference in electronic chemical potential μ of (**1**) and (**2**) and the marginal electrophilic character of (**2**) as predicted by the reactivity indice's analysis.

3.2. Analysis of the CDFT Reactivity Indices of Reactants. Analysis of the DFT-based reactivity indices[67,68] is a very important tool to rationalize the reactivity of polar and ionic reactions in organic chemistry.[80] Hence, an analysis of reactant indices in the gas phase was carried out at the B3LYP/6-311G++(d,p) theory level. The global CDFT reactivity indices[79,81,82] of NO (**1**) and ethylene (**2**) are given in Table 2.

The slight difference of electronic chemical potential μ[79,81,82] indicates that the electron density transfer between reactants (**1**) and (**2**) is not very strong, which expect that the corresponding 32CA reaction has a low polar character, classifying it as of null electron destiny flux (NEDF).[83]

Table 2. B3LYP/6-311++G(d,p) Calculation Level of Global CDFT Reactivity Indices, in eV, of NO (1) and Ethylene (2)

species	μ	η	ω	N
1	−3.77	6.43	1.11	2.50
2	−4.01	5.61	1.43	2.67

The electrophilicity ω index[84] shows that ethylene (**2**) is more electrophilic, 1.43 eV, than NO (**1**), 1.11 eV; while the former is classified as a moderate electrophile, the latter is categorized as a marginal electrophile.[85] However, the nucleophilicity N index[86,87] of (**1**) and (**2**) is close, 2.50 and 2.67 eV, respectively, which allows us to classify them as moderate nucleophiles.[69] Consequently, it will be expected that NO (**1**) participates as a nucleophile and (**2**) as an electrophile in this 32CA reaction. In fact, the moderate electrophilic character of ethylene (**2**), together with the similar electronic chemical potentials, suggests a low polar character and high activation energy for this zw-type 32CA reaction.

3.3. ELF Topological Analysis of NO (1). In order to elucidate the electronic structure of NO (**1**), a topological analysis of the ELF was performed using the Multiwfn program.[88] The basin population analysis in the gas phase shows three V(C1,N2) disynaptic basins, each one integrating 2.04 e and one V(N2,O3) monosynaptic basin of 1.56 e, in addition to three monosynaptic basins on the oxygen atom of 1.91 e, with no basin on the nitrogen atom (Figure 3a,b). These topological features allow classifying NO (**1**) as a zwitterionic TAC[3] (see Figure 3c).

3.4. ELF Study of the 32CA Reaction along the Favored Path of NO (1) with Ethylene (2). Along the reaction path, the ELF topological analysis[70] can also be used as a valuable tool to understand and predict the bonding changes. In order to characterize the C−C and C−O bonding formation between NO (**1**) and ethylene (**2**) in the 32CA reaction, some points of the IRC paths of the most favorable *r*1/*anti* reaction pathway were analyzed. The valence basin populations determined by ELF topological analysis of the some selected points are shown in Tables 3 and 4 and represented in Figure 4a,b, while the corresponding attractor positions associated, essentially, to the two C1−C5 and C4−O3 bond formation are presented in Scheme 3.

From isolated reactants until the point **P1**, no V(C1) monosynaptic basin is observed on NO (**1**), which confirms its zwitterionic structure.

https://doi.org/10.1021/acsomega.4c07794
ACS Omega 2025, 10, 13868−13879

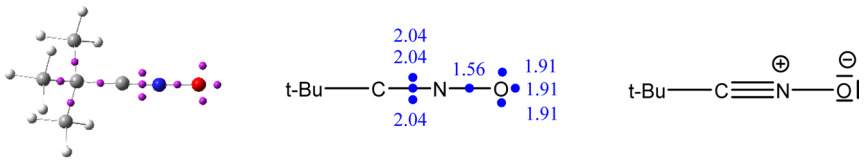

(a) (b) (c)

Figure 3. ELF valence attractor positions (a) and basin populations (b), calculated in the gas phase at the B3LYP/6-311G++(d,p) level, and proposed Lewis-like structure (c) of nitrile oxide (**1**).

Table 3. Bond Lengths, in Angstroms, Å, and Valence Basin Populations, in e, of Selected Structures of *r*1/*anti* Path of the 32CA Reaction between NO and Ethylene in DCM

	P1	P2	P3	TS	P4	P5	P6	P7	CA
ΔE (kcal·mol^{-1})[a]	6.8	16.3	19.8	20.0	18.0	14.1	5.2	−5.4	−30.3
d(C1−C5)	2.845	2.441	2.247	2.197	2.044	1.943	1.801	1.687	1.521
d(C4−O3)	2.855	2.506	2.363	2.328	2.221	2.147	2.025	1.884	1.458
d(O3−H)	2.207	2.180	2.168	2.164	2.154	2.147	2.138	2.131	2.396
V(C1)	0.03	0.64	0.59	0.66					
V(C5)			0.26	0.35					
V(C1,C5)					1.38	1.56	1.76	1.90	2.04
V(C4)						0.12	0.21		
V(O3)							0.21		
V′(O3)	5.75	5.72	5.68	5.70	5.70	5.70	5.50	5.25	4.97
V(C4,O3)								0.77	1.27
V(N2)		1.98	2.23	2.30	2.48	2.57	2.67	2.77	2.93
V(C1,N2)	6.10	3.88	3.86	3.77	3.58	3.49	3.38	3.29	3.15
V(N2,O3)	1.50	1.40	1.34	1.32	1.26	1.23	1.17	1.10	0.96
V(C4,C5)	3.40	3.23	2.91	2.79	2.56	2.35	2.18	2.08	1.95

[a]Relative to reactants (**1** + **2**).

Table 4. Bond Lengths, in Angstroms, Å, and Valence Basin Populations, in e, of Selected Structures of the *r*1/*anti* Path of the 32CA Reaction between NO and Ethylene in Benzene

	P1	P2	P3	TS	P4	P5	P6	P7	CA
ΔE (kcal·mol^{-1})[a]	4.3	14.4	18.5	19.2	18.3	15.5	7.7	1.0	−30.7
d(C1−C5)	2.989	2.491	2.304	2.204	2.103	2.002	1.856	1.769	1.521
d(C4−O3)	2.962	2.530	2.384	2.312	2.240	2.166	2.048	1.960	1.456
d(O3−H)	2.234	2.197	2.185	2.178	2.171	2.164	2.154	2.148	2.378
V(C1)	0.11	0.64	0.61	0.74					
V(C5)			0.25	0.42					
V(C1,C5)					1.38	1.56	1.76	1.85	2.04
V(C4)						0.12	0.22		
V(O3)							0.25		
V′(O3)	5.76	5.69	5.69	5.69	5.69	5.69	5.46	5.29	4.92
V(C4,O3)								0.69	1.27
V(N2)		1.96	2.23	2.35	2.47	2.56	2.68	2.74	2.90
V(C1,N2)	5.92	3.91	3.78	3.70	3.59	3.49	3.38	3.32	3.16
V(N2,O3)	1.53	1.41	1.35	1.31	1.28	1.23	1.18	1.14	0.99
V(C4,C5)	3.41	3.23	2.91	2.70	2.57	2.35	2.18	2.11	1.95

[a]Relative to reactants (**1** + **2**).

In DCM, a monosynaptic basin V(C1) appears at the first point, **P1**, with a slight population of 0.03 e, 6.8 kcal mol^{-1} above reactants. This basin reached 0.64 e (16.3 kcal mol^{-1}) at **P2**, with a new monosynaptic basin V(N2) of 1.98 e appearing on the N2 nitrogen atom and a diminution of the number of disynaptic basins observed in the C1−N2 region from three to two basins. At **P3**, a V(C5) monosynaptic basin of 0.26 e (19.8 kcal mol^{-1}) came into sight. The two monosynaptic basins, V(C1) and V(C5), reach 0.66 and 0.35 e, respectively, at **TS** (20.0 kcal mol^{-1}). The first most suitable change occurs at **P4**, when V(C1) and V(C5) are integrated to give a new disynaptic basin, V(C1,C5), of 1.38 e (18.0 kcal mol^{-1}). These topological changes are associated with the first bond formation of peptides (C1−C5). Next, a V(C4) monosynaptic basin is observed at **P6**, integrating 0.12 e (14.1 kcal mol^{-1}), followed by V(O3) with 0.21 e (5.2 kcal mol^{-1}). The V(O3) monosynaptic basin comes from the V′(O3) monosynaptic basin that is associated with the nonbonding electron density of O3 oxygen atom, which integrates 5.70 e throughout the reaction path before **P6**. The two basins, V(C4) and V(O3), transform into a disynaptic basin V(C4,O3) of 0.77 e (−5.4 kcal mol^{-1}) to form the second single bond (C4−O3). The

https://doi.org/10.1021/acsomega.4c07794
ACS Omega 2025, 10, 13868−13879

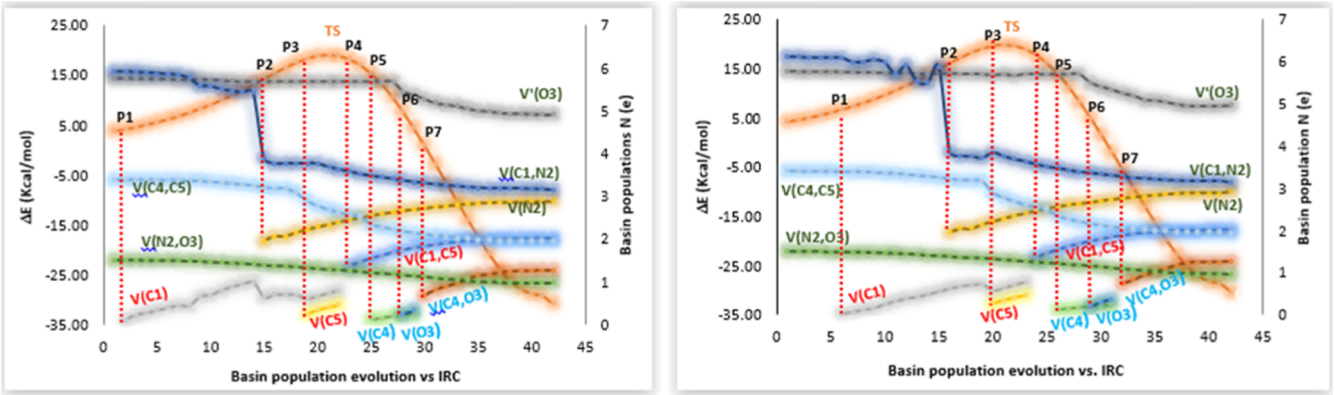

(a): in DCM (b): in benzene

Figure 4. Evolution of the ELF valence basin populations along the favored *r*1/*anti* path.

Scheme 3. ELF Attractor Positions for the Most Relevant Points along the Favored *r*1/*anti* Path of the 32CA Reaction of Nitrile Oxide (1) with Alkene (2)

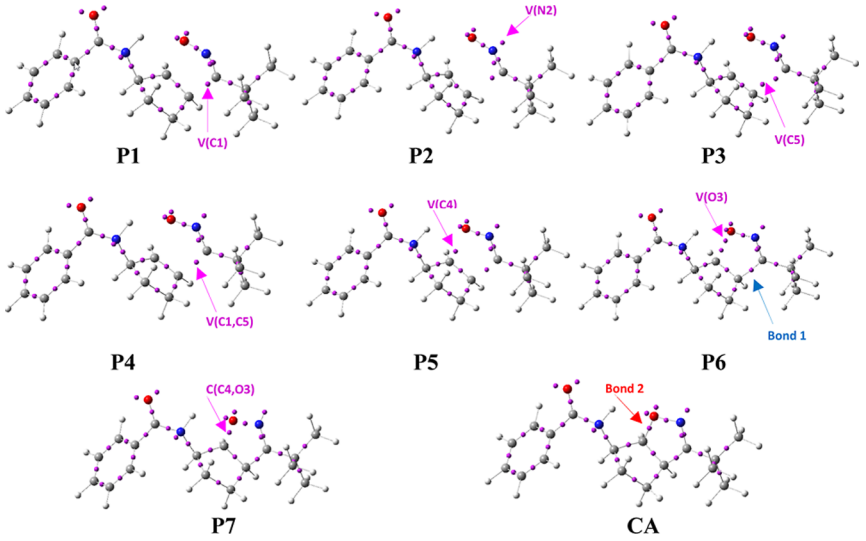

Scheme 4. Molecular Mechanism Representation of the 32CA Reaction Favored Path between NO (1) and Ethylene (2) using ELF Analysis

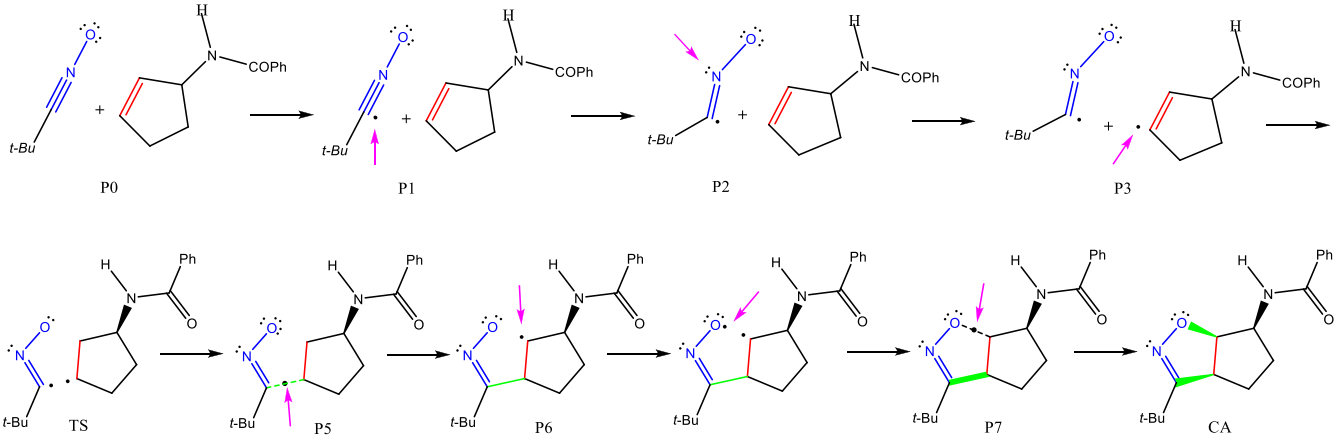

evolution of ELF valence basin populations through the IRC path is given in Figure 4a.

On the other hand, in benzene, the first monosynaptic basin, V(C1), appears with a population of 0.11 e at only 4.3 kcal mol^{-1} above reactants, reaching 0.64 e at **P2** (14.4 kcal mol^{-1}). At this time, a V(N2) monosynaptic basin of 1.96 e is observed at the N2 nitrogen atom with a depopulation of the C−N triple bond from 5.92 to 3.91 e, which implies the transformation of

https://doi.org/10.1021/acsomega.4c07794
ACS Omega 2025, 10, 13868−13879

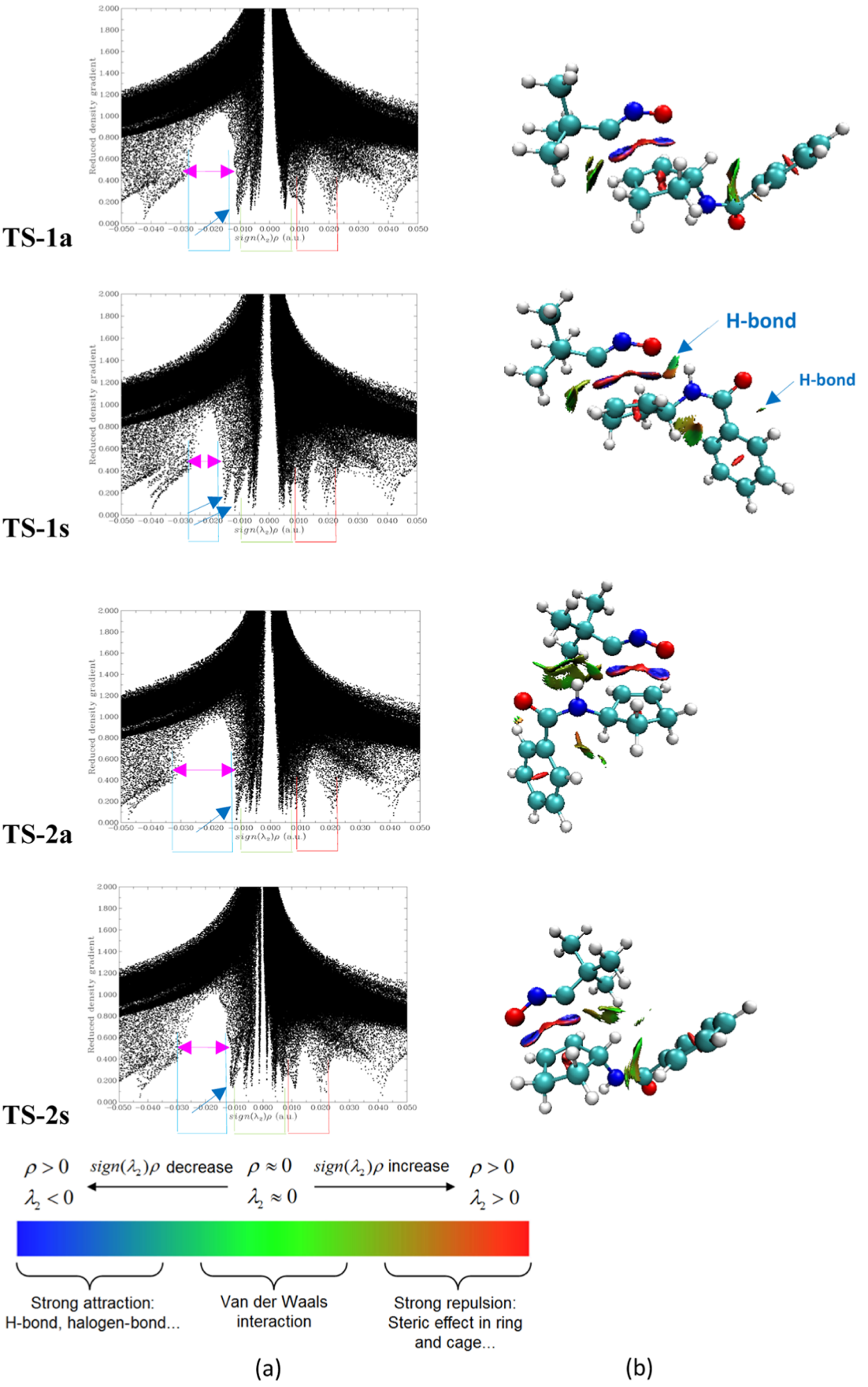

Figure 5. RDG vs sign(λ_2)ρ scatter map (isovalue 0.5) (a) and RDG isosurfaces (isovalue 0.08) (b) of the optimized TSs in the 32CA reaction of NO (**1**) with ethylene (**2**) in the gas phase.

https://doi.org/10.1021/acsomega.4c07794
ACS Omega 2025, 10, 13868−13879

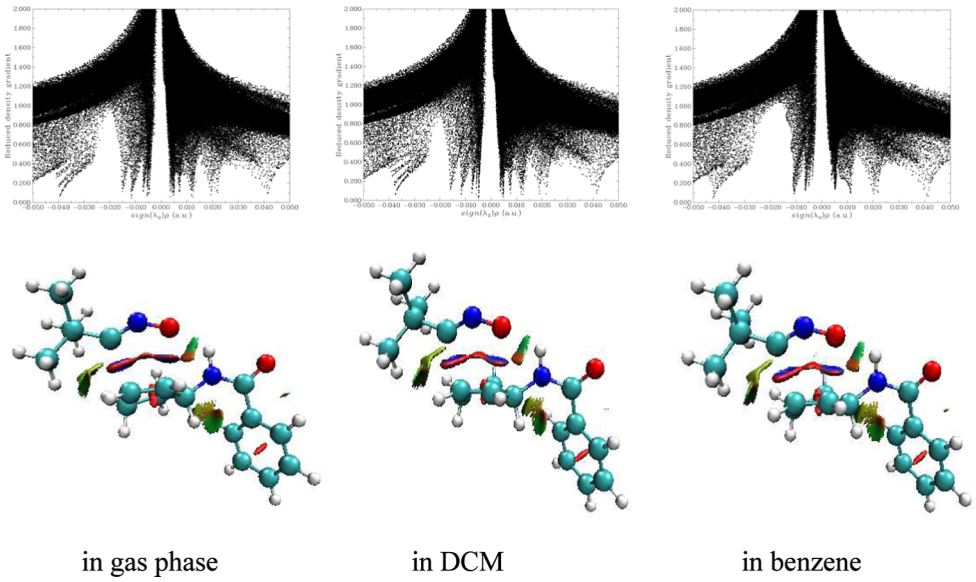

Figure 6. Comparative study of RDG and vs sign(λ_2)ρ scatter map (au) (isovalue 0.5) and RDG isosurfaces (isovalue 0.08) for **TS-1s**.

(**1**) from a propargylic to an allylic structure. At **P3**, a V(C5) monosynaptic basin of 0.25 e (18.5 kcal mol^{-1}) is appeared. The two monosynaptic basins, V(C1) and V(C5), reach 0.74 and 0.42 e, respectively, at **TS** (19.2 kcal mol^{-1}) and merge each other into a disynaptic basin, V(C1,C5), integrating 1.38 e (18.3 kcal mol^{-1}) at **P4**. These topological changes are associated with the formation of the first single bond (C1−C5). At **P5**, a V(C4) monosynaptic basin is observed with a population of 0.12 e (15.5 kcal mol^{-1}), followed by a V(O) monosynaptic basin with a population of 0.25 e (7.7 kcal mol^{-1}) at **P6**. The two basins merge each other, forming a new V(C4,O3) disynaptic basin of 0.69 e (1.0 kcal mol^{-1}) to form the second single bond (C4−O3). The evolution of ELF valence basin populations through the IRC path is given in Figure 4b.

The most relevant finding from this ELF study is the significant evolution in basin populations with a decrease in energy in benzene compared to the reaction in DCM (Tables 3 and 4), which explains why the 32CA reaction between NO (**1**) and ethylene (**2**) is better realized in benzene than in DCM (see Table 1). However, mechanistically, no significant changes are observed.

This ELF topological analysis allowed us to propose the following mechanism of this reaction (Scheme 4).

Along the reaction path, the disynaptic basins in the C1−N2 region of NO (**1**) experience a depopulation due to its participation in the density formation of the lone pairs at the N2 atom and a pseudoradical center[89] at the C1 carbon of the NO, leading to the first C1−C5 bond formation. The second bond, O3−C4, is formed by sharing the nonbonding electron density of the oxygen of NO and the C4 pseudoradical center created after the formation of the first C1−C5 bond. As can be seen in Figure 4, the O3−C4 and C1−C5 bond formation takes place in notably separated points of the IRC, which accounts for the asynchronous bond formation. In fact, the second bond forms when the first is almost completed, suggesting a nonpolar two-stage one-step mechanism.

3.5. Hydrogen Bond and NCI Analysis in TSs.

3.5.1. NCI Analysis of TSs in the Gas Phase. The NCI[75] is a very applied method to study the weak interactions. In order to characterize the hydrogen bond effect on the selectivity of the 32CA reaction, the NCI method is used. The scatter maps of the NCI of the 32CA reaction of NO (**1**) and ethylene (**2**) for all optimized TSs in the gas phase are given in Figure 5a, while the corresponding RDG isosurfaces are shown in Figure 5b. In the graphs (Figure 5a), the *X*-axis represents the sign(λ_2)ρ function, while the *Y*-axis represents the RDG one. Note that the plot of the NCI attractive region (left region) at **TS-1s** shows two spikes and a denser region compared to those of **TS-1a**, **TS-2s**, and **TS-2a**, which show one spike and a less dense region. The repulsive (right region) and weak interactive regions (center region) show more spikes for all TSs, indicating more repulsive NCIs like steric interactions associated with the benzene ring of (**2**) and the *t*-butyl group of (**1**). Therefore, both the darker green surface between the NO oxygen and the amide hydrogen at **TS-1s** (see Figure 5b), and the additional spike found at the attractive region in the corresponding plot, show the presence of a weak hydrogen bond, which leads to the stronger stabilization of **TS-1s** compared to the other TSs and subsequently to the observed *r*1/*syn* selectivity.

*3.5.2. NCI Analysis of **TS-1s** in Solvents.* In Figure 6, the scatter map plots the gas phase, and DCM and benzene are represented and compared. The repulsive NCI (red region) and weak interaction (green region) of **TS-1s** indicate more spikes in the gas phase and in DCM than in benzene. On the other side, the attractive region shows a denser spike in benzene compared to DCM, representing the H-bond, which is clearly shown by RDG isosurfaces (Figure 6). These findings might suggest that **TS-1s** can be more selective in benzene relative to DCM, which confirm energy calculations given in Table 1 (see above).

4. CONCLUSIONS

The present study provides evidence of the important role played by hydrogen bonding and solvent effects in orienting regio- and stereoselectivities of the 32CA reactions between 2,2-dimethylpropanenitrile oxide (**1**) and *N*-(cyclopent-2-en-1-yl)benzamide (**2**). The reactivity has been rationalized using MEDT at the B3LYP/6-311++G(d,p) level. The computed activation and reaction Gibbs free energies show that the *r*1/

https://doi.org/10.1021/acsomega.4c07794
ACS Omega 2025, 10, 13868−13879

syn isomeric path, via **TS-1s**, leading to the formation of the **CA-1s** cycloadduct, is the most favored path both in DCM and in benzene, with a slight decrease of energy using benzene as the solvent, which is in good agreement with experimental results. The ELF topological analysis clearly shows the zwitterionic structure of NO (**1**) participating in the zw-type 32CA reactions. The present reaction follows a mechanism in one step. The electronic chemical potentials of the reagents at the ground state predict a nonpolar reaction character, which is confirmed by the calculated GEDT in the TSs. The creation of the two new σ-bonds, C−C and C−O, is described using ELF topological analysis of basin and population evolution along the more favored *r*1/*syn* reaction path in solvents. The presence of an H-bond between the oxygen of NO (**1**) and the amide hydrogen of ethylene (**2**) in the favored **TS-1s**, allows proving its effect on the selectivity of this 32CA reaction, as predicted by Curran et al. in 1990. Using the NCIs method, the analysis of scatter maps and RDG-isosurfaces, in the gas phase and in both solvents, shows a weak attractive interaction N−H···O, being responsible for the *r*1/*syn* selectivity.

This MEDT study permits us to explain the regio- and stereoselectivity experimentally observed and to propose a plausible mechanism of the 32CA reaction between 2,2-dimethylpropanenitrile oxide and *N*-(cyclopent-2-en-1-yl)-benzamide.

This work opens a path to extend the 32CA reaction study at theoretical and experimental levels. The other nitrones and dipolarophiles will be considered in future studies to understand whether the observed mechanistic details are generally applicable. In addition, further extending the computational methods to account for explicit solvent effects or other DFT functionals may also improve the predictions of the selectivity and reactivity. Furthermore, the potential bioactivity of the cycloadducts suggests an avenue for future studies.

■ ASSOCIATED CONTENT

Supporting Information

The Supporting Information is available free of charge at https://pubs.acs.org/doi/10.1021/acsomega.4c07794.

Total energies and Gibbs free energies calculated at the B3LYP/6-311++G(d,p) level in the gas phase, in DCM, and in benzene of the stationary points involved in the 32CA reactions between 2,2-dimethylpropanenitrile oxide (**1**) and *N*-(cyclopent-2-en-1-yl)benzamide (**2**), as well as profiles representing the four competitive reaction paths (PDF)

■ AUTHOR INFORMATION

Corresponding Authors

Sofiane Benmetir − *Process and Environmental Engineering Laboratory (LIPE), Faculty of Chemistry, University of Science and Technology of Oran Mohamed BOUDIAF, 31000 Oran, Algeria; Department of Physical Chemistry, Faculty of Pharmacy, University of Valencia, 46100 Valencia, Spain;* orcid.org/0000-0002-2492-2750; Email: sofiane.benmetir@univ-usto.dz

Haydar Mohammad-Salim − *Faculty of Science, Department of Chemistry, University of Zakho, Duhok 42001 Kurdistan Region, Iraq; Molecular Topology and Drug Design Research Unit and Department of Physical Chemistry, Faculty of Pharmacy, University of Valencia, 46100 Valencia, Spain;* orcid.org/0000-0002-9600-3446; Email: hayder.salim@uoz.edu.krd

Authors

Lakhdar Benhamed − *Laboratory of Applied Thermodynamics and Molecular Modeling (LAT2M), Department of Chemistry, Faculty of Science, University of Tlemcen, Tlemcen 13000, Algeria*

Noureddine Tchouar − *Process and Environmental Engineering Laboratory (LIPE), Faculty of Chemistry, University of Science and Technology of Oran Mohamed BOUDIAF, 31000 Oran, Algeria*

Jesús Vicente de Julián-Ortiz − *Department of Physical Chemistry, Faculty of Pharmacy, University of Valencia, 46100 Valencia, Spain*

Mar Ríos-Gutiérrez − *Department of Organic Chemistry, University of Valencia, 46100 Valencia, Spain;* orcid.org/0000-0001-8894-2710

Luis R. Domingo − *Department of Organic Chemistry, University of Valencia, 46100 Valencia, Spain;* orcid.org/0000-0002-2023-0108

Complete contact information is available at: https://pubs.acs.org/10.1021/acsomega.4c07794

Notes

The authors declare no competing financial interest.

■ ACKNOWLEDGMENTS

J. V. de J.-O. acknowledges the University of Valencia - Special Activities grant UV-INV_AE-3677056 for financial support. The authors also dedicate this work to the memory of Professor Jorge Galvez who devoted his life to research and scientific development in the drug design field.

■ REFERENCES

(1) Smith, L. I. Aliphatic Diazo Compounds, Nitrones, Compounds, Structurally Analogous Systems Capable of Undergoing 1, 3-Additions. *Chem. Rev.* **1938**, *23* (2), 193−285.

(2) Huisgen, R. 1,3-dipolar cycloadditions. Past and future. *Angew. Chem., Int. Ed. Engl.* **1963**, *2* (10), 565−598.

(3) Ríos-Gutiérrez, M.; Domingo, L. R. Unravelling the mysteries of the [3 + 2] cycloaddition reactions. *Eur. J. Org Chem.* **2019**, *2019* (2−3), 267−282.

(4) Jäger, V.; Colinas, P. A. Nitrile oxides. In *Synthetic Applications of 1,3-Dipolar Cycloaddition Chemistry Toward Heterocycles and Natural Products*; Wiley, 2002; Vol. *59*, pp 361−472.

(5) Huisgen, R. 1.3-Dipolare Cycloadditionen Rückschau und Ausblick. *Angew. Chem.* **1963**, *75* (13), 604−637.

(6) Jasiński, R.; Żmigrodzka, M.; Dresler, E.; Kula, K. A Full Regioselective and Stereoselective Synthesis of 4-Nitroisoxazolidines via Stepwise [3 + 2] Cycloaddition Reactions between (Z)-C-(9-Anthryl)-N-arylnitrones and (E)-3, 3, 3-Trichloro-1-nitroprop-1-ene: Comprehensive Experimental and Theoretical Study. *J. Heterocycl. Chem.* **2017**, *54* (6), 3314−3320.

(7) Łapczuk-Krygier, A.; Kącka-Zych, A.; Kula, K. Recent progress in the field of cycloaddition reactions involving conjugated nitroalkenes. *Curr. Chem. Lett.* **2019**, *8* (1), 13−38.

(8) Fryźlewicz, A.; Łapczuk-Krygier, A.; Kula, K.; Demchuk, O. M.; Dresler, E.; Jasiński, R. Regio- and stereoselective synthesis of nitrofunctionalized 1,2-oxazolidine analogs of nicotine. *Chem. Heterocycl. Compd.* **2020**, *56*, 120−122.

(9) Zhang, P.-Z.; Li, X.-L.; Chen, H.; Li, Y.-N.; Wang, R. The synthesis and biological activity of novel spiro-isoxazoline C-disaccharides based on 1,3-dipolar cycloaddition of exo-glycals and sugar nitrile oxides. *Tetrahedron Lett.* **2007**, *48* (44), 7813−7816.

(10) Jasiński, R.; Dresler, E. On the question of zwitterionic intermediates in the [3 + 2] cycloaddition reactions: A critical review. *Organics* **2020**, *1* (1), 49−69.
(11) Grundmann, C.; Grünanger, P. *The Nitrile Oxides*; Springer Verlag Berlin: Heidelberg-New York, NY, 1971; Vol. *141*, p 161.
(12) Torssell, K. B. G. *Nitrile Oxides, Nitrones, and Nitronates in Organic Synthesis: Novel Strategies in Synthesis*; VCH: Weinheim, 1988.
(13) Feuer, H. *Nitrile Oxides, Nitrones and Nitronates in Organic Synthesis: Novel Strategies in Synthesis*; John Wiley & Sons, 2008.
(14) Caramella, P.; Grünanger, P. *1,3-Dipolar Cycloaddition Chemistry*; Wiley-Interscience: New York, 1984; Vol. *1*.
(15) Easton, C. J.; Hughes, C. M. M.; Savage, G. P.; Simpson, G. W. Cycloaddition reactions of nitrile oxides with alkenes. *Adv. Heterocycl. Chem.* **1994**, *60*, 261−327.
(16) (a) Chikkula, K. V.; Raja, S. Isoxazole − a potent pharmacophore. *Int. J. Pharm. Pharm. Sci.* **2017**, *9*, 13−24. (b) Wang, X.; Hu, Q.; Tang, H.; Pan, X. Isoxazole/Isoxazoline Skeleton in the Structural Modification of Natural Products: A Review. *Pharmaceuticals* **2023**, *16* (2), 228.
(17) Alegaon, S. G.; Alagawadi, K. R.; Garg, M. K.; Dushyant, K.; Vinod, D. 1,3,4-Trisubstituted pyrazole analogues as promising anti-inflammatory agents. *Bioorg. Chem.* **2014**, *54*, 51−59.
(18) Joseph, L.; George, M. Evaluation of in vivo and in vitro anti-inflammatory activity of novel isoxazole series. *Eur. Int. J. Sci. Technol.* **2016**, *5* (3), 35−42.
(19) Umesha, B.; Basavaraju, Y. B. Synthesis and characterization of novel benzo [d][1,3] dioxole gathered pyrazole derivatives and their antimicrobial evaluation. *Med. Chem. Res.* **2014**, *23*, 3744−3751.
(20) (a) Pol, S.; Kadam, V.; Ramesh, B.; Mali, S. S.; Patil, V. Synthesis and Evaluation of isoxazole for their antimicrobial activity. *IP Int. J. Compr. Adv. Pharmacol.* **2017**, *2*, 19−26. (b) Wang, J.; Wang, D.-B.; Sui, L.-L.; Luan, T. Natural products-isoxazole hybrids: A review of developments in medicinal chemistry. *Arabian J. Chem.* **2024**, *17* (6), 105794.
(21) Nagamallu, R.; Srinivasan, B.; Ningappa, M. B.; Kariyappa, A. K. Synthesis of novel coumarin appended bis (formylpyrazole) derivatives: Studies on their antimicrobial and antioxidant activities. *Bioorg. Med. Chem. Lett.* **2016**, *26* (2), 690−694.
(22) (a) Ahmad, A.; Ahmad, A.; Varshney, H.; Rauf, A.; Rehan, M.; Subbarao, N.; Khan, A. U. Designing and synthesis of novel antimicrobial heterocyclic analogs of fatty acids. *Eur. J. Med. Chem.* **2013**, *70*, 887−900. (b) Bąchor, U.; Brożyna, M.; Junka, A.; Chmielarz, M. R.; Gorczyca, D.; Mączyński, M. Novel Isoxazole-Based Antifungal Drug Candidates. *Int. J. Mol. Sci.* **2024**, *25* (24), 13618.
(23) Ren, J.; Wang, S.; Ni, H.; Yao, R.; Liao, C.; Ruan, B. Synthesis, Characterization and Antitumor activity of novel ferrocene-based amides bearing pyrazolyl moiety. *J. Inorg. Organomet. Polym. Mater.* **2015**, *25*, 419−426.
(24) Hamama, W.; Ibrahim, M.; Zoorob, H. Synthesis and biological evaluation of some novel isoxazole derivatives. *J. Heterocycl. Chem.* **2017**, *54* (1), 341−346.
(25) Fioravanti, R.; Desideri, N.; Biava, M.; Droghini, P.; Atzori, E. M.; Ibba, C.; Collu, G.; Sanna, G.; Delogu, I.; Loddo, R. N-((1,3-Diphenyl-1H-pyrazol-4-yl) methyl) anilines: a novel class of anti-RSV agents. *Bioorg. Med. Chem. Lett.* **2015**, *25* (11), 2401−2404.
(26) Li, F.; Hu, Y.; Wang, Y.; Ma, C.; Wang, J. Expeditious lead optimization of isoxazole-containing influenza A virus M2-S31N inhibitors using the Suzuki−Miyaura cross-coupling reaction. *J. Med. Chem.* **2017**, *60* (4), 1580−1590.
(27) Prajapti, S. K.; Shrivastava, S.; Bihade, U.; Gupta, A. K.; Naidu, V. G. M.; Banerjee, U. C.; Babu, B. N. Synthesis and biological evaluation of novel Δ^2-isoxazoline fused cyclopentane derivatives as potential antimicrobial and anticancer agents. *MedChemComm* **2015**, *6* (5), 839−845.
(28) Pinho e Melo, T. M. Recent advances on the synthesis and reactivity of isoxazoles. *Curr. Org. Chem.* **2005**, *9* (10), 925−958.
(29) El-Sehemi, A. G.; Bondock, S.; Ammar, Y. A. Transformations of naproxen into pyrazolecarboxamides: Search for potent anti-inflammatory, analgesic and ulcerogenic agents. *Med. Chem. Res.* **2014**, *23*, 827−838.
(30) Karabasanagouda, T.; Adhikari, A. V.; Girisha, M. Synthesis of some new pyrazolines and isoxazoles carrying 4-methylthiophenyl moiety as potential analgesic and antiinflammatory agents. *Indian J. Chem.* **2009**, *48B*, 430−437.
(31) (a) Krompiec, S.; Lodowski, P.; Kurpanik-Wójcik, A.; Gołek, G.; Mieszczanin, A.; Fijołek, A.; Matussek, M.; Kaszuba, K. Nitrile Oxide, Alkenes, Dipolar Cycloaddition, Isomerization and Metathesis Involved in the Syntheses of 2-Isoxazolines. *Molecules* **2023**, *28* (6), 2547. (b) Song, X.; Wang, H.; Gao, Y.; Xu, K.; Sun, Z.; Zhao, C.; Yao, G.; Xu, H. Design, synthesis, and evaluation of novel isoxazoline derivatives containing 2-phenyloxazoline moieties as potential insecticides. *Pestic. Biochem. Physiol.* **2024**, *204*, 106109.
(32) Mohammad-Salim, H. A.; Acharjee, N.; Domingo, L. R.; Abdallah, H. H. A molecular electron density theory study for [3 + 2] cycloaddition reactions of 1-pyrroline-1-oxide with disubstituted acetylenes leading to bicyclic 4-isoxazolines. *Int. J. Quantum Chem.* **2021**, *121* (5), No. e26503.
(33) Zawadzińska, K.; Kula, K. Application of *β*-Phosphorylated Nitroethenes in [3 + 2] Cycloaddition Reactions Involving Benzonitrile N-Oxide in the Light of a DFT Computational Study. *Organics* **2021**, *2* (1), 26−37.
(34) Zeroual, A.; Ríos-Gutiérrez, M.; Salah, M.; El Alaoui El Abdallaoui, H.; Ramon Domingo, L. An investigation of the molecular mechanism, chemoselectivity and regioselectivity of cycloaddition reaction between acetonitrile N-Oxide and 2,5-dimethyl-2H-[1,2,3]-diazaphosphole: a MEDT study. *J. Chem. Sci.* **2019**, *131* (8), 75.
(35) Zawadzińska, K.; Ríos-Gutiérrez, M.; Kula, K.; Woliński, P.; Mirosław, B.; Krawczyk, T.; Jasiński, R. The Participation of 3,3,3-Trichloro-1-nitroprop-1-ene in the [3 + 2] Cycloaddition Reaction with Selected Nitrile N-Oxides in the Light of the Experimental and MEDT Quantum Chemical Study. *Molecules* **2021**, *26* (22), 6774.
(36) Ríos-Gutiérrez, M.; Domingo, L. R.; Esseffar, M.; Oubella, A.; Ait Itto, M. Y. Unveiling the Different Chemical Reactivity of Diphenyl Nitrilimine and Phenyl Nitrile Oxide in [3 + 2] Cycloaddition Reactions with (R)-Carvone through the Molecular Electron Density Theory. *Molecules* **2020**, *25* (5), 1085.
(37) Abdullah, H.; Opoku, E. Quantum chemical analysis of the molecular mechanism and selectivity of the 32CA reaction of nitrile oxides with 5-(ethylthio) furan-2(5H)-ones and N-substituted-2-azanorborn-5-ene. *Comput. Theor. Chem.* **2023**, *1229*, 114324.
(38) Kula, K.; Zawadzińska, K. Local nucleophile-electrophile interactions in [3 + 2] cycloaddition reactions between benzonitrile N-oxide and selected conjugated nitroalkenes in the light of MEDT computational study. *Curr. Chem. Lett.* **2021**, *10*, 9−16.
(39) Mondal, A.; Acharjee, N. Unveiling the exclusive stereo and site selectivity in [3 + 2] cycloaddition reactions of a tricyclic strained alkene with nitrile oxides from the molecular electron density theory perspective. *Chem. Heterocycl. Compd.* **2023**, *59* (3), 145−154.
(40) Kula, K.; Łapczuk-Krygier, A. A DFT computational study on the [3 + 2] cycloaddition between parent thionitrone and nitroethene. *Curr. Chem. Lett.* **2018**, *7*, 27−34.
(41) Kula, K.; Dobosz, J.; Jasiński, R.; Kącka-Zych, A.; Łapczuk-Krygier, A.; Mirosław, B.; Demchuk, O. [3 + 2] Cycloaddition of diaryldiazomethanes with (E)-3,3,3-trichloro-1-nitroprop-1-ene: An experimental, theoretical and structural study. *J. Mol. Struct.* **2020**, *1203*, 127473.
(42) Domingo, L. R.; Emamian, S.; Salami, M.; Ríos-Gutiérrez, M. Understanding the molecular mechanism of the [3 + 2] cycloaddition reaction of benzonitrile oxide toward electron-rich N-vinylpyrrole: a DFT study. *J. Phys. Org. Chem.* **2016**, *29* (7), 368−376.
(43) Ndassa, I. M.; Adjieufack, A. I.; Mbadcam Ketcha, J.; Berski, S.; Ríos-Gutiérrez, M.; Domingo, L. R. Understanding the reactivity and regioselectivity of [3 + 2] cycloaddition reactions between substituted nitrile oxides and methyl acrylate. A molecular electron density theory study. *Int. J. Quantum Chem.* **2017**, *117* (24), No. e25451.

https://doi.org/10.1021/acsomega.4c07794
ACS Omega 2025, 10, 13868−13879

(44) Domingo, L. R. Molecular Electron Density Theory: A Modern View of Reactivity in Organic Chemistry. *Molecules* **2016**, *21* (10), 1319.
(45) Ríos-Gutiérrez, M.; Domingo, L. R. Unravelling the Mysteries of the [3 + 2] Cycloaddition Reactions. *Eur. J. Org Chem.* **2019**, *2019* (2−3), 267−282.
(46) Domingo, L. R.; Acharjee, N. Molecular Electron Density Theory: A New Theoretical Outlook on Organic Chemistry. *Front. Comput. Chem.* **2020**, *5*, 174−227.
(47) Curran, D. P.; Choi, S. M.; Gothe, S. A.; Lin, F. T. Directed nitrile oxide cycloaddition reactions. The use of hydrogen bonding to direct regio- and stereochemistry in nitrile oxide cycloadditions with cyclopentenylamides. *J. Org. Chem.* **1990**, *55* (12), 3710−3712.
(48) Lee, C.; Yang, W.; Parr, R. G. Development of the Colle-Salvetti correlation-energy formula into a functional of the electron density. *Phys. Rev. B:Condens. Matter Mater. Phys.* **1988**, *37* (2), 785−789.
(49) Becke, A. D. Density functional thermochemistry. III. The role of exact exchange. *J. Chem. Phys.* **1993**, *98* (7), 5648−5652.
(50) Wiberg, K. B. Ab Initio Molecular Orbital Theory by W. J. Hehre, L. Radom, P. v. R. Schleyer, and J. A. Pople, John Wiley, New York, 548pp. *J. Comput. Chem.* **1986**, *7* (3), 379.
(51) Frisch, M. J.; Trucks, G. W.; Schlegel, H. B.; Scuseria, G. E.; Robb, M. A.; Cheeseman, J. R.; Scalmani, G.; Barone, V.; Mennucci, B.; Petersson, G. A.; Nakatsuji, H.; Caricato, M.; Li, X.; Hratchian, H. P.; Izmaylov, A. F.; Bloino, J.; Zheng, G.; Sonnenberg, J. L.; Hada, M.; Ehara, M.; Toyota, K.; Fukuda, R.; Hasegawa, J.; Ishida, M.; Nakajima, T.; Honda, Y.; Kitao, O.; Nakai, H.; Vreven, T.; Montgomery, J. A.; Peralta, J. E.; Ogliaro, F.; Bearpark, M.; Heyd, J. J.; Brothers, E.; Kudin, K. N.; Staroverov, V. N.; Kobayashi, R.; Normand, J.; Raghavachari, K.; Rendell, A.; Burant, J. C.; Iyengar, S. S.; Tomasi, J.; Cossi, M.; Rega, N.; Millam, J. M.; Klene, M.; Knox, J. E.; Cross, J. B.; Bakken, V.; Adamo, C.; Jaramillo, J.; Gomperts, R.; Stratmann, R. E.; Yazyev, O.; Austin, A. J.; Cammi, R.; Pomelli, C.; Ochterski, V.; Martin, R. L.; Morokuma, K.; Zakrzewski, V. G.; Voth, G. A.; Salvador, P.; Dannenberg, J. J.; Dapprich, S.; Daniels, A. D.; Farkas, O.··.; Foresman, J. B.; Ortiz, J. V.; Cioslowski, J.; Fox, D. J. *Gaussian 09*. Revision A.1; Gaussian, Inc.: Wallingford CT, 2009.
(52) Schlegel, H. B. Optimization of equilibrium geometries and transition structures. *J. Comput. Chem.* **1982**, *3* (2), 214−218.
(53) Schlegel, H. B. Geometry Optimization on Potential Energy Surfaces. In *Modern Electronic Structure Theory*; Yarkony, D. R., Ed.; World Scientific Publishing: Singapore, 1994; Vol. *2*.
(54) Legault, C. CYLview 2.0. 2019. www.cylview.org.
(55) Gonzalez, C.; Schlegel, H. B. Reaction Path Following in Mass-Weighted Internal Coordinates. *J. Phys. Chem.* **1990**, *94*, 5523−5527.
(56) Gonzalez, C.; Schlegel, H. B. Improved algorithms for reaction path following: Higher-order implicit algorithms. *J. Chem. Phys.* **1991**, *95* (8), 5853−5860.
(57) Fukui, K. Formulation of the reaction coordinate. *J. Phys. Chem.* **1970**, *74* (23), 4161−4163.
(58) Gupta, M.; Silva, E. F. d.; Svendsen, H. F. Computational Study of Thermodynamics of Polyamines with Regard to CO_2 Capture. *Energy Procedia* **2012**, *23*, 140−150.
(59) Simkin, B. I. A.; Sheĭkhet, I. I. Quantum chemical and statistical theory of solutions: a computational approach. In *Ellis Horwood series in physical chemistry*; Ellis Horwood: London, 1995.
(60) Tomasi, J.; Mennucci, B.; Cammi, R. Quantum Mechanical Continuum Solvation Models. *Chem. Rev.* **2005**, *105* (8), 2999−3094.
(61) Cancès, E.; Mennucci, B.; Tomasi, J. A new integral equation formalism for the polarizable continuum model: Theoretical background and applications to isotropic and anisotropic dielectrics. *J. Chem. Phys.* **1997**, *107* (8), 3032−3041.
(62) Cossi, M.; Barone, V.; Cammi, R.; Tomasi, J. Ab initio study of solvated molecules: a new implementation of the polarizable continuum model. *Chem. Phys. Lett.* **1996**, *255* (4), 327−335.
(63) Barone, V.; Cossi, M.; Tomasi, J. Geometry optimization of molecular structures in solution by the polarizable continuum model. *J. Comput. Chem.* **1998**, *19* (4), 404−417.
(64) Domingo, L. R. A new C−C bond formation model based on the quantum chemical topology of electron density. *RSC Adv.* **2014**, *4* (61), 32415−32428.
(65) Reed, A. E.; Weinstock, R. B.; Weinhold, F. Natural population analysis. *J. Chem. Phys.* **1985**, *83* (2), 735−746.
(66) Reed, A.; Curtiss, L.; Weinhold, F. Intermolecular Interactions from a Natural Bond Orbital, Donor-Acceptor Viewpoint. *Chem. Rev.* **1988**, *88*, 899−926.
(67) Parr, R. G.; Yang, W. *Density Functional Theory of Atoms and Molecules*; Oxford University Press: New York, 1989.
(68) Domingo, L. R.; Ríos-Gutiérrez, M.; Pérez, P. Applications of the conceptual density functional theory indices to organic chemistry reactivity. *Molecules* **2016**, *21* (6), 748.
(69) Domingo, L. R.; Ríos-Gutiérrez, M.; Pérez, P. Applications of the Conceptual Density Functional Theory Indices to Organic Chemistry Reactivity. *Molecules* **2016**, *21* (6), 748.
(70) Lu, T.; Chen, F. Multiwfn: A multifunctional wavefunction analyzer. *J. Comput. Chem.* **2012**, *33* (5), 580−592.
(71) Savin, A.; Becke, A. D.; Flad, J.; Nesper, R.; Preuss, H.; von Schnering, H. G. A New Look at Electron Localization. *Angew Chem. Int. Ed. Engl.* **1991**, *30* (4), 409−412.
(72) Silvi, B.; Savin, A. Classification of chemical bonds based on topological analysis of electron localization functions. *Nature* **1994**, *371* (6499), 683−686.
(73) Savin, A.; Silvi, B.; Colonna, F. Topological analysis of the electron localization function applied to delocalized bonds. *Can. J. Chem.* **1996**, *74* (6), 1088−1096.
(74) Savin, A.; Nesper, R.; Wengert, S.; Fässler, T. F. ELF: The Electron Localization Function. *Angew Chem. Int. Ed. Engl.* **1997**, *36* (17), 1808−1832.
(75) Contreras-García, J.; Johnson, E. R.; Keinan, S.; Chaudret, R.; Piquemal, J.-P.; Beratan, D. N.; Yang, W. NCIPLOT: a program for plotting non-covalent interaction regions. *J. Chem. Theory Comput.* **2011**, *7* (3), 625−632.
(76) Pagenkopf, B. L. Synthetic Applications of 1,3-Dipolar Cycloaddition Chemistry Toward Heterocycles and Natural Products Edited by A. Padwa (Emory University) and W. H. Pearson (University of Michigan). Wiley-Interscience. *J. Nat. Prod.* **2004**, *67*, 1074.
(77) Giernoth, R. Solvents and Solvent Effects in Organic Chemistry. 4th Ed. By Christian Reichardt and Thomas Welton. *Angew. Chem., Int. Ed.* **2011**, *50* (48), 11289.
(78) Benchouk, W.; Mekelleche, S. M.; Silvi, B.; Aurell, M. J.; Domingo, L. R. Understanding the kinetic solvent effects on the 1,3-dipolar cycloaddition of benzonitrile N-oxide: a DFT study. *J. Phys. Org. Chem.* **2011**, *24* (7), 611−618.
(79) Domingo, L. R.; Ríos-Gutiérrez, M.; Pérez, P. A molecular electron density theory study of the participation of tetrazines in aza-Diels−Alder reactions. *RSC Adv.* **2020**, *10* (26), 15394−15405.
(80) Liu, S. *Conceptual Density Functional Theory: Towards a New Chemical Reactivity Theory*; Wiley-VCH GmbH, 2022.
(81) Parr, R. G.; Pearson, R. G. Absolute hardness: companion parameter to absolute electronegativity. *J. Am. Chem. Soc.* **1983**, *105* (26), 7512−7516.
(82) Calais, J. L. Density-functional theory of atoms and molecules. R.G. Parr and W. Yang, Oxford University Press, New York, Oxford, 1989. *Int. J. Quantum Chem.* **1993**, *47* (1), 101.
(83) Domingo, L. R.; Ríos Gutiérrez, M. A useful classification of organic reactions based on the flux of the electron density. *Sci. Radices* **2023**, *2* (1), 1−24.
(84) Parr, R. G.; Szentpály, L. V.; Liu, S. Electrophilicity Index. *J. Am. Chem. Soc.* **1999**, *121* (9), 1922−1924.
(85) Ríos-Gutiérrez, M.; Saz Sousa, A.; Domingo, L. R. Electrophilicity and nucleophilicity scales at different DFT computational levels. *J. Phys. Org. Chem.* **2023**, *36* (7), No. e4503.
(86) Domingo, L. R.; Chamorro, E.; Pérez, P. Understanding the Reactivity of Captodative Ethylenes in Polar Cycloaddition Reactions. A Theoretical Study. *J. Org. Chem.* **2008**, *73* (12), 4615−4624.

https://doi.org/10.1021/acsomega.4c07794
ACS Omega 2025, 10, 13868−13879

(87) Domingo, L.; Pérez, P. The nucleophilicity N index in organic chemistry. *Org. Biomol. Chem.* **2011**, *9*, 7168−7175.
(88) Lu, T.; Chen, F. Multiwfn: a multifunctional wavefunction analyzer. *J. Comput. Chem.* **2012**, *33* (5), 580−592.
(89) Domingo, L. R.; Sáez, J. A. Understanding the electronic reorganization along the nonpolar [3 + 2] cycloaddition reactions of carbonyl ylides. *J. Org. Chem.* **2011**, *76* (2), 373−379.

https://doi.org/10.1021/acsomega.4c07794
ACS Omega 2025, 10, 13868−13879